Biochimica et Biophysica Acta 1828 (2013) 1036–1046

Contents lists available at SciVerse ScienceDirect

Biochimica et Biophysica Acta

journal homepage: www.elsevier.com/locate/bbamem

Approximate calculation and experimental derivation of native isoelectric points of membrane protein complexes of *Arabidopsis* chloroplasts and mitochondria

Christof Behrens [a], Kristina Hartmann [b,1], Stephanie Sunderhaus [a], Hans-Peter Braun [a], Holger Eubel [a,*]

[a] Institute for Plant Genetics, Faculty of Natural Sciences, Leibniz University of Hannover, Germany
[b] Gelcompany GmbH, Tübingen, Germany

ARTICLE INFO

Article history:
Received 13 February 2012
Received in revised form 16 November 2012
Accepted 20 November 2012
Available online 29 November 2012

Keywords:
Membrane protein complexes
Ionisable amino acids
Native isoelectric point
Mitochondria
Chloroplasts
Free flow electrophoresis

ABSTRACT

Electric charges are important intrinsic properties of proteins. They directly affect functionality and also mediate interactions with other molecules such as cofactors, substrates and regulators of enzymatic activity, with lipids as well as other proteins. As such, analysis of the electric properties of proteins gives rise to improved understanding of the mechanism by which proteins fulfil their specific functions. This is not only true for singular proteins but also applies for defined assemblies of proteins, protein complexes and supercomplexes. Charges in proteins often are a consequence of the presence of basic and acidic amino acid residues within polypeptide chains. In liquid phase, charge distributions of proteins change in response to the pH of their environment. The interdependence of protein charge and the surrounding pH is best described by the isoelectric point, which is notoriously difficult to obtain for native protein complexes. Here, experimentally derived native isoelectric points (npIs) for a range mitochondrial and plastid protein complexes are provided. In addition, for four complexes, npIs were calculated by a novel approach which yields results largely matching the experimental npIs.

1. Introduction

The charges generated by the ionisable proteinogenic amino acids cysteine, aspartic acid, glutamic acid, histidine, lysine, arginine and tyrosine have profound impacts on protein function and activity. These amino acids are not distributed evenly within proteins but concentrate on or near the surface of native proteins where interaction with the liquid phase takes place [1]. There, they mediate binding of ligands to proteins [2,3], promote protein complex:protein complex interactions [4], influence the structural integrity and stability of proteins [5,6], and anchor proteins to membranes [7]. In other positions, ionisable amino acids are also involved in enzymatic activity [1,8] and in transport processes [9]. Analysing occurrence and distribution of ionisable amino acids in proteins therefore delivers valuable information on physico-chemical attributes important for their biological function.

Since ionisable amino acids are amphoteric, their charge state depends on the pH of the solvent. Consequently, for proteins, the pH at which their net charge becomes zero (its isoelectric point, pI) is determined by the influence of the pH on the entity of their ionisable amino acids. By definition, pIs describe the properties of whole proteins or protein complexes and cannot be used for the prediction of events taking place in spatially limited areas of the protein surface. Nevertheless, establishing the pI of a native protein or protein complex (npI) can deliver valuable information on the bulk properties of ionisable amino acids. For example, knowledge about pIs can be used to predict the subcellular locations of proteins [10]. It also allows gaining information on the pH of their cellular environment. Proteins are poorly dissolved in media with pH values similar to the proteins npI since this would decrease their solubility. Practical applications benefitting from the analysis of the npI include the engineering of active sites [11] and, more importantly, the successful production of protein crystals for x-ray structural analyses [12,13].

Commonly, bioinformatic approaches are the preferred options in ascertaining npIs since experimental analysis often is difficult and time-consuming. Driven by the widespread use of isoelectric focussing in multidimensional protein separation, calculation of pIs of denatured proteins is now well established and delivers accurate results [14]. Such calculations are based on experimentally acquired values for acid dissociation constants (pK_a) [15,16] which are applied to all ionisable

Abbreviations: AMPSO, N-(1,1-Dimethyl-2-hydroxyethyl)-3-amino-2-hydroxypropanesulfonic acid; BN, blue-native; CMC, critical micellar concentration; ESI, electro spray ionisation; FFE, free-flow electrophoresis; HEPES, 4-(2-Hydroxyethyl) piperazine-1-ethanesulfonic acid; HPMC, (Hydroxypropyl)methyl cellulose; ICS, intercristal space; IEF, isoelectric focussing; LC, liquid chromatography; LHCII, light-harvesting complex II; MS, mass-spectrometry; nIEF, native isoelectric focussing; npI, native isoelectric point; OPM, Orientation of Proteins in Membranes database; OXPHOS, oxidative phosphorylation; PAGE, polyacrylamide gel electrophoresis; PDB, Protein Data Bank; pI, isoelectric point; SPADNS, 2-(4-Sulfophenylazo)-1,8-dihydroxy-3,6-naphthalenedisulfonic acid; TOF, time of flight

* Corresponding author at: Leibniz University of Hannover, Institute for Plant Genetics, Department of Plant Proteomics, Herrenhäuser Strasse 2, 30419 Hannover, Germany. Tel.: +49 5117622699; fax: +49 5117623608.
E-mail address: heubel@genetik.uni-hannover.de (H. Eubel).
[1] Present address: Assign International GmbH, München-Martinsried, Germany.

0005-2736/$ – see front matter © 2012 Elsevier B.V. All rights reserved.
http://dx.doi.org/10.1016/j.bbamem.2012.11.028

amino acid residues found within a polypeptide chain. However, employing this approach for the calculation of pIs under non-denaturing (i.e. native) conditions is difficult due to protein folding. While relatively rare, some of the ionisable residues are buried deep inside the proteins [17], where they form hydrogen bonds or may become subject to desolvation events and charge-charge interactions. Therefore, their pK_a values tend to be different from those residues which are located on the water accessible surface of the protein [18]. Ideally, the pK_a value of every single ionisable amino acid is determined individually in order to establish the native pI of a protein. However, especially in case of high molecular mass proteins or protein complexes, this approach simply is not feasible. Direct measurement of pK_a values within a native protein is difficult and, to date, can only be performed on small and midsized proteins [19]. Several different approaches rely on empirical methods ([20] and [21]), or more sophisticated modelling techniques using continuum electrostatics [22–25]. Quality of the predictions varies between the individual approaches and often the null model (the use of predefined pK_a values for all ionisable amino acids) or empirical approaches outperform more sophisticated approaches [19,26]. The aim of this study is to experimentally determine and to calculate native pIs of the large membrane protein complexes and supercomplexes involved in photosynthesis and respiration. Data density on the native pI of these energetically so important protein complexes is low. Unfortunately, most of the above-mentioned approaches are deemed unreasonable for this use due to the sheer size of these complexes and the high number of ionisable amino acid requiring immense calculation power if, for example, performed by a continuum electrostatics approach. Therefore, this study promotes a simple, easy-to-use approach for the rough calculation of native pIs of membrane protein complexes of plant mitochondria and chloroplasts. For this, pK_a values defined by Henriksson and co-workers [27] on experimentally derived npIs of native proteins were used for a modified null model. However, only water accessible, ionisable residues are considered for this approach whereas the difficult-to-predict, buried ionisable amino acids are ignored. This requires structural information on protein complexes and, in case of membrane complexes, knowledge of their exact position within their harbouring membranes.

Calculated npIs are complemented by experimental results obtained from carefully solubilised protein complexes subsequently analysed by gel-free isoelectric focussing using Free-Flow Electrophoresis (IEF-FFE). The prevailing model plant Arabidopsis was chosen for this study because of its frequent use for genetic and biochemical studies in plant research. Unfortunately, the status of Arabidopsis as the prevailing model organism is not reflected by the number of available protein structures. This required the calculations to be based on information derived on homologous protein complexes. From non-Arabidopsis protein complex structures deposited in the Protein Database (PDB), water accessible ionisable amino acids positioned at the surface of the respective native Arabidopsis membrane proteins were deduced. Exemplarily, npIs for the chloroplast light-harvesting complex II (LHCII), the dimeric mitochondrial cytochrome bc_1 complex (complex III_2) and the F_1 ATP-synthase subcomplexes of mitochondria and chloroplasts were calculated.

Comparison of the data from the predictive and experimental approaches and cross-comparison with other published data demonstrates that the modified null model chosen for npI calculations as well as FFE isoelectric focussing are practical approaches for the determination of native isoelectric points yielding reliable results.

2. Results and discussion

2.1. Identification of water exposed amino acids in the Arabidopsis LHCII trimer

Due to the lack of X-ray structures of the Arabidopsis LHCII trimer, data of the closest homolog with available structural data were chosen to identify the positions of ionisable amino acids within the Arabidopsis protein complexes. For the LHC trimer, ionisable amino acids were first located in the corresponding structure of *Pisum sativum* [4] (Fig. 1A) using the open source 'Java' based viewer 'Jmol' [28]. According to the localisation data stored in the 'Orientations of Proteins in Membranes' (OPM) database [29], ionisable residues cluster on the stromal and luminal sides of the complex and only few reside in the trans-membrane regions (Fig. 1B). In order to distinguish ionisable residues which are water accessible from those which are buried inside the complex, a water-accessible surface was modelled in Jmol using a 1.4 Å diameter probe. Since this is a purely qualitative approach including also residues which are only partly accessible to water, the degree of surface-exposure of all ionisable residues was predicted employing the Netsurf1.1 algorithm of Petersen et al. [30]. All subunits were processed separately and every residue above the exposure threshold of 25% was included in the analyses.

Transfer of the results obtained on the pea LHCII trimer onto the corresponding Arabidopsis homolog was achieved by aligning amino acid sequences of LHCb1–3 of Arabidopsis and the LHCb1 of pea (Suppl. Fig. 1). Sequence similarity between all LHCb homologs of both species was found to be high with 56% overall sequence identity and only 24% non-conserved substitutions [31]. Furthermore, the three major Arabidopsis LHCII homologs share a 58% sequence identity and a 77% sequence similarity, suggesting similar three-dimensional

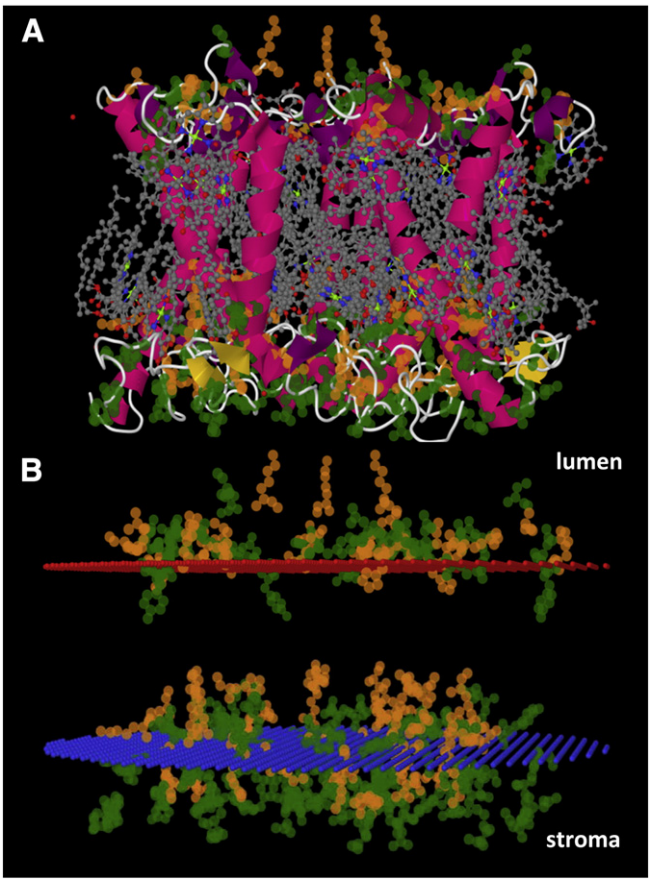

Fig. 1. Structure of the LHCII of *Pisum sativum* [4]. A, side view of the complete protein complex; B, side view of ionisable amino acids only and their location in relation to the thylakoid membrane. Perspective in A and B is from the plane of the membrane. Green spheres, atoms of acidic amino acid residues (cysteine, aspartic acid, glutamic acid, tyrosine); orange spheres, atoms of basic amino acid residues (histidine, lysine, arginine). A: Secondary structures are indicated by purple helices or white strings; coloured dots, non-protein atoms. B: Red layer, lumenal surface side of thylakoid membrane; blue layer, stromal surface side of thylakoid membrane.

structures [32] and spatial distributions of amino acids. Therefore, also the numbers of exposed ionisable amino acid residues on the stroma and lumen exposed sides in pea and the Arabidopsis isoforms are expected to be similar. Moreover, LHCII heterotrimers of Arabidopsis composed of different amounts of LHCb1–3 proteins should also possess structures similar to the LHCb1 homotrimer of pea. Since most of the surface exposed ionisable amino acid residues are located in fully conserved or highly similar regions, comparable patterns seem likely in Arabidopsis. Consequently, the ionisable pea residues were used for the calculation of npI in Arabidopsis with good confidence. Chloroplast transit peptides are rich in positively charged amino acids and therefore can be expected to exert a considerable influence on the pIs of organellar proteins. Using TargetP1.1 [33], the length of the signal peptides was predicted and, in a last step, their ionisable amino acids were excluded from the calculations of npIs.

An overview of the quantities and distributions of ionisable amino acids within the LHCb proteins of pea and Arabidopsis is presented in Suppl. Table 2. The high similarities in amino acid sequences are also reflected by the overall number of exposed ionisable amino acids and their distribution over the luminal and stromal surfaces. Approximately half of these residues are exposed to the stroma or lumen-facing surfaces allowing them to interact with the aqueous chloroplast compartments. Analysis of the ionisable residues in cyclodextrin glycosyltransferase, an enzyme consisting of a similar number of amino acids as trimeric LHCII, produced a similar ratio of water exposed to water inaccessible ionisable amino acids [34], indicating a reasonable outcome also for our calculations on LHCII.

2.2. Identification of water exposed amino acids in the Arabidopsis dimeric cytochrome c reductase complex (complex III_2)

While the calculations for trimeric LHCII were relatively simple due to the symmetrical layout of the complex and the availability of X-ray structures from a closely related species, the situation for respiratory complex III is more difficult (Fig. 2). Lack of a plant complex III crystal structure requires the use of structural data on the bovine protein complex. Unfortunately, the structure of the best dimeric mitochondrial complex III from *Bos taurus* (PDB ID: 1pp9) [35] is missing a 6.4 kDa subunit, which needed to be substituted by the subunit of a different structure of bovine complex III (PDB ID: 1l0l) [36]. In contrast to the high homology of LHCII subunits between pea and Arabidopsis, complex III subunits from mammals share a level of identity of approximately only 30% to 60% with higher plants (here: potato [37]). This is partly due to the transit peptide of the Rieske iron sulphur protein remaining attached to the bovine complex III after cleavage. As such, it can be regarded as a de facto subunit. Therefore, the functional dimeric form of complex III consists of 20 subunits in Arabidopsis [38] but 22 subunits in beef [39,40]. Despite this, all subunits of Arabidopsis complex III were successfully aligned with their beef counterparts (Suppl. Fig. 2). Using OPM [29] data, the distribution of ionisable residues in the complex and their exposure to either the matrix or the intermembrane space was calculated in the same fashion as outlined for the LHCII trimer. These results are summarised in Suppl. Table 3. Similar to the LHCII trimer, only few ionisable amino acids are located in the transmembrane region while the bulk is facing the IMS or matrix orientated surfaces of the complex (Fig. 2B).

2.3. Identification of water exposed amino acids in the Arabidopsis F_1 ATP-synthase of mitochondria and chloroplasts

In addition to the membrane-located LHCII and complex III, npIs for the soluble F_1 parts of the F_1F_O ATP-synthases of Arabidopsis mitochondria and chloroplasts were calculated. Detailed structural data for plant F_1 ATP synthase is scarce and in general, only α and β subunits are resolved well (e.g. in PDB ID: 1fx0, [41]). To circumvent this lack of high quality structural data, the yeast mitochondrial structure (PDB ID: 2xok) [42] was used for the identification of ionisable amino acids in the Arabidopsis mitochondrial as well as chloroplast F_1 ATP-synthase. In contrast to its F_O part, the yeast F_1 sub-complex with a subunit composition of $\alpha_3\beta_3\gamma_1\delta_1\varepsilon_1$ (Fig. 3A) is available at a resolution suitable for detecting ionisable amino acids in this structure. A subunit stoichiometry of $\alpha_3\beta_3\gamma_1\delta_1\varepsilon_1$ for F_1 of plant mitochondria and chloroplasts is commonly accepted [43] and was consequently used for our predictions.

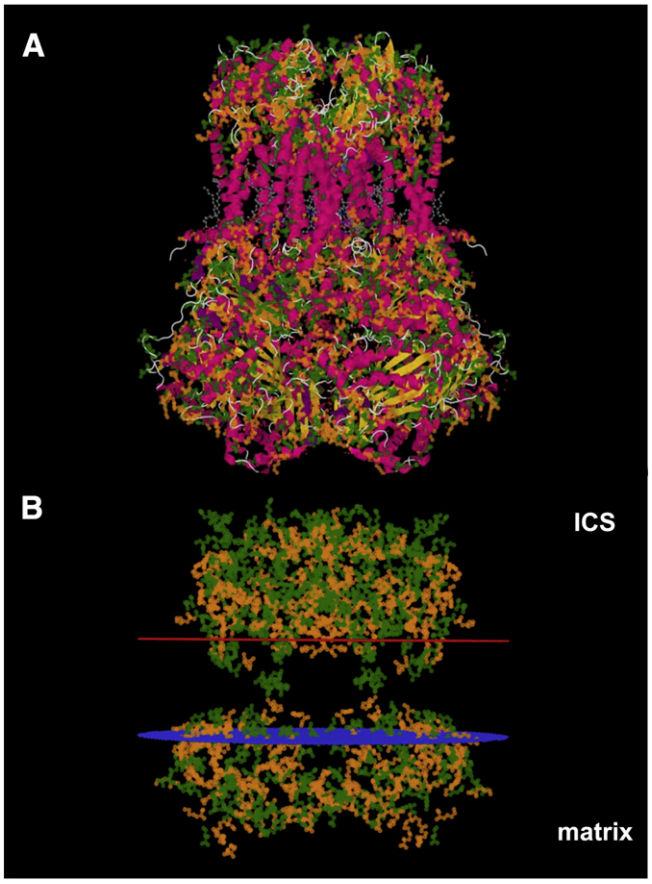

Fig. 2. Structure of the bovine complex III [35]. A, side view of the complete protein complex; B, side view of ionisable amino acids only and their location in relation to the inner mitochondrial membrane. Perspective in A and B is from the plane of the membrane. The 6.4 kDa subunit is missing in this representation. Green spheres, atoms of acidic amino acid residues (cysteine, aspartic acid, glutamic acid, tyrosine); orange spheres, atoms of basic amino acid residues (histidine, lysine, arginine). A: Secondary structure is indicated by purple helices, yellow beta sheets or white strings; coloured dots, non-protein atoms. B: Red layer, intercristal space exposed surface of the inner mitochondrial membrane; blue layer, matrix exposed side of inner mitochondrial membrane. Subunits without transmembrane regions and the 6.4 kDa subunit are omitted in B.

The sequence alignment of subunits of yeast and Arabidopsis mitochondrial F_1 ATP-synthase after removal of transit peptides (Suppl. Table 1) revealed a high homology (Suppl. Fig. 3), which is reflected in the distribution of ionisable amino acid residues exposed to the mitochondrial matrix (Suppl. Table 4). The same situation was found for the alignments of yeast α, β and γ subunits with their respective chloroplast homologs. However, alignment of δ and ε required more efforts. Mitochondrial δ-subunit shows higher similarity to the chloroplast (and bacterial) ε-subunit than with the chloroplast δ-subunit ([44], Suppl. Fig. 4). The subunit homologous to bacterial/chloroplast δ, the mitochondrial oligomycin-sensitivity-conferring protein (OSCP) [45] is actually missing in the structures of yeast F_1 and was replaced by subunit δ from *E. coli* for the alignments of yeast mitochondrial and Arabidopsis chloroplastic F_1

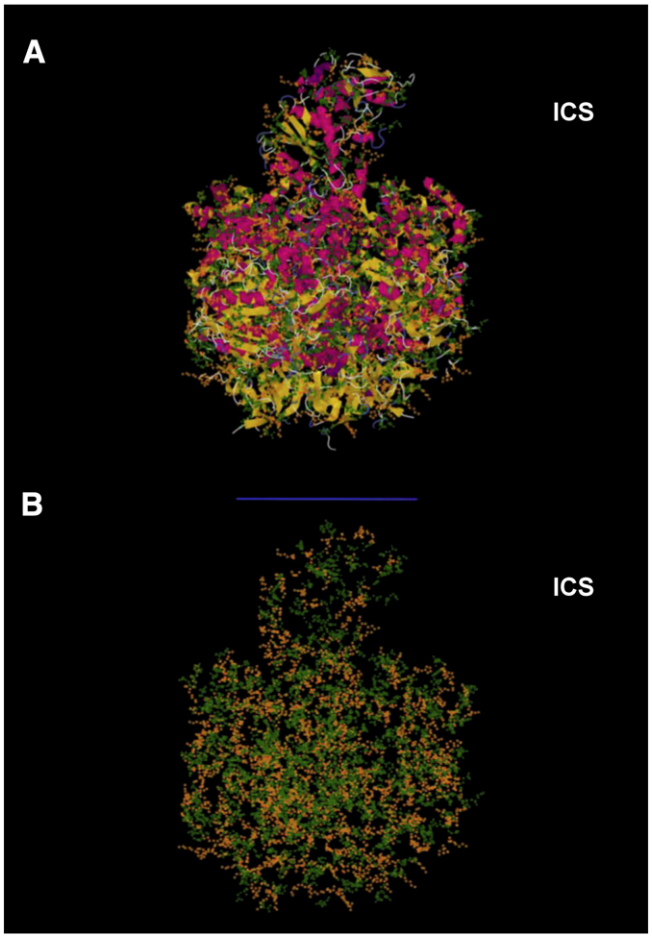

Fig. 3. Structure of the yeast mitochondrial F_1F_0 ATP-synthase [42]. A, side view of the F_1-part; B, side view of ionisable amino acids only and their location in relation to the matrix oriented side of inner mitochondrial membrane. The rotor of the F_o-part of ATP-synthase consisting of 10 copies of subunit c also included in the structure is not shown. Perspective in A and B is from the plane of the membrane. Green spheres, atoms of acidic amino acid residues (cysteine, aspartic acid, glutamic acid, tyrosine); orange spheres, atoms of basic amino acid residues (histidine, lysine, arginine). A: Secondary structure is indicated by purple helices, yellow beta sheets or white strings; coloured dots, non-protein atoms. B: blue layer, matrix exposed side of inner mitochondrial membrane.

ATP-synthase. For the spatial distribution of ionisable residues it was assumed that all solvent-accessible ionisable residues are embedded in the stroma of chloroplasts (Suppl. Table 4).

2.4. Approximate calculation of theoretical npIs

The data on ionisable amino acid localisation and distribution in Arabidopsis LHCII, complex III and F_1 ATP-synthase of chloroplasts and mitochondria were then used to predict the native pIs of both membrane protein complexes and the two F_1 ATP-synthase subcomplexes. Two different sets of pK_a values were used for this. The first set was developed for pI calculation of denatured proteins with the EMBOSS software package [46]. In contrast, the pK_a values in set two were optimised for the calculation of native proteins by Henriksson and co-workers [27]. Computation of npIs based on the Hendersson–Hasselbalch equation was performed using the self-developed "nativepI" tool (http://www.genetik.uni-hannover.de/nativepI.html), which uses parts of a source code described elsewhere [47]. In contrast to other software, nativepI is capable of handling multiple N and C-termini which is mandatory when dealing with protein complexes. With both sets of pK_a values, native pIs were calculated using either all ionisable amino acids of the protein complexes or using water-accessible amino acid residues only (Table 1, Suppl. Fig. 5). Since the Arabidopsis LHCII trimer may consist of different isoforms of LHCb [31,48,49] predictions of npIs were done for the three most abundant combinations (Table 1).

Noticeably, compared to those using only the surface exposed residues, npIs of the LHCII trimers are always higher when all ionisable amino acids are considered. Also, predictions based on the pK_a values of Henriksson et al. [27] generally yield lower npIs compared to the predictions based on the pK_a values of EMBOSS [46]. This latter observation is most likely caused by the lower pK_a values for most ionisable groups by Henriksson and co-workers. Without any exception, native pIs derived from the calculations using only the surface exposed residues have the lowest value.

To evaluate the approach outlined here against established methods, we used PROPKA2.0 [50] as the benchmark for an independent calculation of npIs of pea LHCII trimer, bovine complex III and yeast F_1 ATP-synthase. PROPKA2.0 has been rated high in recent comparisons of pK_a prediction approaches [19,51] and also uses structural information from the PDB (here: PDB IDs: 2bhw and 1pp9). It considers protein ligands for the calculations which might be advantageous in the case of the chlorophyll containing trimeric LHCII complex. As outlined previously, it is expected that the high sequence identity of pea and Arabidopsis LHCII results in similar outputs while the lower degree in homology between complex III of beef and Arabidopsis may produce more diverging values. The npIs predicted by PROPKA2.0 exceeded even the sequence based prediction results obtained with both sets of pK_a values. The only exception to this is the npI of Arabidopsis complex III calculated with the pK_a values of EMBOSS, which is slightly higher than the PROPKA2.0 value. However, since some side-chain atoms were missing (lysine at position 91 and glutamic acid at position 107 in all three chains of PDB ID: 2bhw; tyrosine 223 and glutamic acid 225 in chain A and N and glutamic acid 39 and tyrosine 78 in chain I and V of PDB ID: 1pp9) an accurate prediction with PROPKA2.0 was not possible and npIs had to be estimated from the titration curve provided by the software. In any case, the missing 6.4 kDa subunit in the structure of bovine complex III seems to have only minor effects on the npI calculation since it contains only a small number of ionisable amino acids. For mitochondrial F_1 ATP-synthase of yeast npI calculation by PROPKA 2.0 was hampered by missing atoms in the crystal structure of the complex (glutamic acid at position 56 and 198, lysine at position 58 and aspartic acid at position 200 in chain G, glutamic acid at position

Table 1
Predicted native isoelectric points of LHCII trimer isoforms and dimeric complex III of *Arabidopsis*.

	PROPKA2.0[a]	pK_a EMBOSS[b]		pK_a Henriksson[c]	
		All	Water accessible surface	All	Water accessible surface
LHCb1, 1, 1[d]	5.4	4.77	4.55	4.59	4.37
LHCb1, 1, 2[d]	n/a	4.76	4.46	4.59	4.27
LHCb1, 2, 3[d]	n/a	4.67	4.19	4.47	3.89
Complex III_2	6.5	6.65	5.99	6.18	5.60
F1-ATP-synthase (mitochondrial)	6.5	5.61	4.71	5.55	4.56
F1-ATP-synthase (chloroplast)	6.5	5.06	4.83	4.95	4.70

[a] Structure based prediction for pea trimeric LHCII (PDB ID: 2bhw), bovine dimeric complex III (PDB ID: 1pp9) and yeast F1 ATP-synthase (PDB-ID: 2xok) using PROPKA2.0 [50].
[b] Prediction of Arabidopsis npIs with nativepI using the pK_a values of EMBOSS [46] including all ionisable residues or surface exposed ionisable residues.
[c] Prediction of Arabidopsis npIs with nativepI using the pK_a values of Henriksson et al. [27] including all ionisable residues or surface exposed ionisable residues.
[d] Light harvesting II timers composed of three copies of the LHCb1 isoform, two copies of the LHCb1 form and one copy of LHCb2 or one copy of LHCb1, LHCb2 and LHCb3.

26, 50, 95, 99, 107, 119, 122, 128 and 131, lysine at position 35, 66, 67, 102, 109 and 110 and arginine at position 118 in chain H, glutamic acid at position 55, lysine at position 48 and 61 and arginine at position 22 in chain I of PDB ID: 2xok). Its npI therefore had to be estimated by using the titration curve given by PROPKA 2.0 in the same fashion as outlined for bovine complex III. Additionally, the rotor consisting of 10 c-subunits in the yeast F_o subcomplex was automatically included in the PROPKA 2.0 prediction, probably accounting for most of the considerable difference between the predicted values of PROPKA2.0 and native pI.

2.5. Experimental analyses of the npIs of Arabidopsis chloroplast and mitochondrial protein complexes and supercomplexes

Since npI values for the LHCII trimer and mitochondrial complex III differed strongly between the calculations employing different pK_a sets, npIs of protein complexes of chloroplast and mitochondria were investigated experimentally using free flow electrophoresis (FFE). FFE (reviewed by Islinger et al. [52]) provides a matrix-free, continuous separation and is often used for isolation of organelles [53–57]. When used for IEF, FFE of native proteins does not suffer from typical problems encountered with hydrophobic proteins, such as aggregation and precipitation [58]. For the determination of mitochondrial and chloroplast protein complex npIs, a pH 2 - 8 gradient was selected since it comfortably covers the range of all predicted npIs. For solubilisation of mitochondrial and chloroplast protein complexes prior to FFE, the non-ionic detergent digitonin was chosen because it preserves the native state of plastid and mitochondrial membrane protein complexes and supercomplexes [38,59]. Unlike other detergents, digitonin also has the added advantage of not disturbing IEF. Since those ionisable residues of a membrane protein which are in vivo covered by the lipid bilayer will be shielded by the detergent micelle after solubilisation, the npIs of solubilised membrane protein complexes is expected to resemble that of membrane inserted complexes. Digitonin was also added to the separation medium at a concentration above its critical micellar concentration (CMC) to avoid precipitation of proteins during FFE.

After native IEF-FFE (nIEF-FFE), fractions were analysed on blue-native (BN) gels [60]. Separation patterns of the complexes of both organelles are distinct (Figs. 4 and 5). Protein complexes were identified by comparing their electrophoretic mobility in BN-PAGE with that of known patterns of digitonin-solubilised samples directly submitted to BN-PAGE [38,59]. In total, biological replicates for 3 chloroplast samples and 2 mitochondrial samples were submitted to the FFE treatment (Suppl. Figs. 6 and 7). Based on amido black protein quantitation, it is estimated that ~75% of the injected protein was recovered from the FFE fractions. No precipitation of sample material was observed during the run (data not shown). From the sample injection point at pH 5.4, nearly all chloroplast and mitochondrial protein complexes migrate towards the acidic range of the gradient and only a few complexes focus at more basic pH values. Streaking of complexes over several fractions is common but the exact reasons for this are unclear (see next section for detailed discussion of this point). Despite obvious streaking, peak FFE fractions could always be identified. The pH values of these peak fractions were taken as the npIs of the mitochondrial and chloroplast protein complexes and supercomplexes.

In general, npIs of chloroplast complexes (for reviews of chloroplast protein complexes and supercomplexes see [49,61,62]) are more acidic compared to the mitochondrial ones (Figs. 4 and 5). The two largest PSII supercomplexes ($C_2S_2M_2$, 1300 kDa; C_2S_2M/C_2SM_2; 1150 kDa) have npIs ranging from 3.79 to 4.97 and share a peak npI of 4.25. The slightly smaller C_2S_2/C_2SM supercomplex (1000 kDa) has a more basic migration pattern (pI 4.01 - 4.98), peaking at 4.36. The npIs of photosystem I-containing supercomplexes covered the range of pH 3.95–5.03 (PSI + LHCI + LHCII) and pH 3.92–5.26 (PSI + LHCI) respectively. While the peak of the PSI + LHCI supercomplex is observed at pH 4.67, the centre npI of photosystem I with a single LHCII attached (PSI + LHCI + LHCII) is found at a more acidic pH of 4.50. The npI of the F_1-part of chloroplastic ATP synthase and photosystem II core ranged from pH 4.20 to 5.05 with a peak at pH 4.63, and for the cytochrome b_6f (pH 4.84–5.65) the central fraction was found at pH 5.12. The peak npI of trimeric LHCII lies at pH 4.17, ranging from pH 3.66 to pH 4.59.

For complexes and supercomplexes smaller than 600 kDa, these results are in agreement with experimentally derived npIs for Arabidopsis LHCII (pH 4.0 - 4.10) [48] and spinach (pH 4.20 - 4.42) [63] derived from non-denaturing IEF-PAGE. Matrix-free IEF of thylakoid membrane complexes of spinach performed by D'Amici et al. [64] in a multi-chamber electrophoresis system allowed the determination of the npI for LHCII of 3.85 to 4.31. Furthermore, npIs of 4.62 ± 0.18 for PSI + LHCI supercomplex and cytochrome b_6f were also reported. No complex larger than the PSI + LHCI (560 kDa) was observed, probably due to the solubilisation conditions (i.e. the detergent of choice) employed in these studies. With digitonin, PSII supercomplexes up to 1300 kDa [59] remained intact during BN-PAGE. Protein complexes with molecular masses and stoichiometries similar to those observed in BN-PAGE have also been detected after FFE, suggesting that the native state of the protein complexes under FFE-conditions is not compromised.

For the mitochondrial protein complexes and supercomplexes (for a review of mitochondrial protein complexes and supercomplexes see [65]), peak npIs ranging from 4.77 to 5.44 can be observed (Fig. 5, Table 2). As in the chloroplast samples, the major mitochondrial protein complexes found on BN/SDS- gels [38] are also present in the FFE-fractions. Again, this indicates conditions preserving the native state of the complexes in nIEF-FFE. A protein supercomplex with a molecular weight of 1500 kDa remained intact during FFE separation and is clearly visible on BN-PAGE. Similar to chloroplasts, some streaking of all (super-) complexes is evident in the mitochondrial fractions. In detail, the $I + III_2$ supercomplex is observed in fractions covering ph 4.85–5.36 with a peak npI of 5.07. Complex I also possess a peak npI of 5.07 and shows streaking behaviour comparable to the supercomplex (pH 4.81–5.47). Dimeric complex III is distributed in fractions covering the pH range of 4.48–5.43, while the peak npI is observed at 4.92. The Heat-shock protein 60 complex ranging from pH 4.50 to 4.98 peaks at 4.77. Complex V, the mitochondrial ATPase and its F_1-Part subcomplex have comparable peak npIs of 5.44 (complex V) and 5.31 (F_1-Part), respectively, while their npIs range from 4.88 to 5.82 (F_1-part) and 5.00 to 5.83 (complex V).

Peak broadening of protein complexes in BN-PAGE of FFE fractions — in vivo distributions of protein complex charges or experimental artefacts?
Potential reasons for the observed 'streaking' of protein complex bands in BN-PAGE of the FFE fractions are manifold and include biological as well as technical reasons:

- Protein complexes carry hundreds, if not thousands of charges and their subunits are subject to protein modifications which potentially introduce additional charges to the complex.
- Solubilisation of protein complexes is a critical step in the experimental approach for analysing native pIs described here. Detergent strength and concentration affect the degree to which lipids (from the membrane or intrinsic) are removed from the protein complex.
- Compromised FFE-performance might have led to incomplete focussing.
- In some cases, two or more different protein complexes of the same molecular mass but slightly different npI might give the impression of smearing in BN-PAGE of FFE fractions
- The native state of protein complexes might not be preserved to the same level in FFE and BN-PAGE, leading to a partial breakdown of high-molecular-mass associations in the latter due to higher mechanical stress in this system. This would also explain the presence of several different complexes within the same FFE-fraction.

Considering the amount of charges present within protein complexes, it seems unlikely that every single copy of such a complex will have exactly the same charge. Modifications of subunits, be it

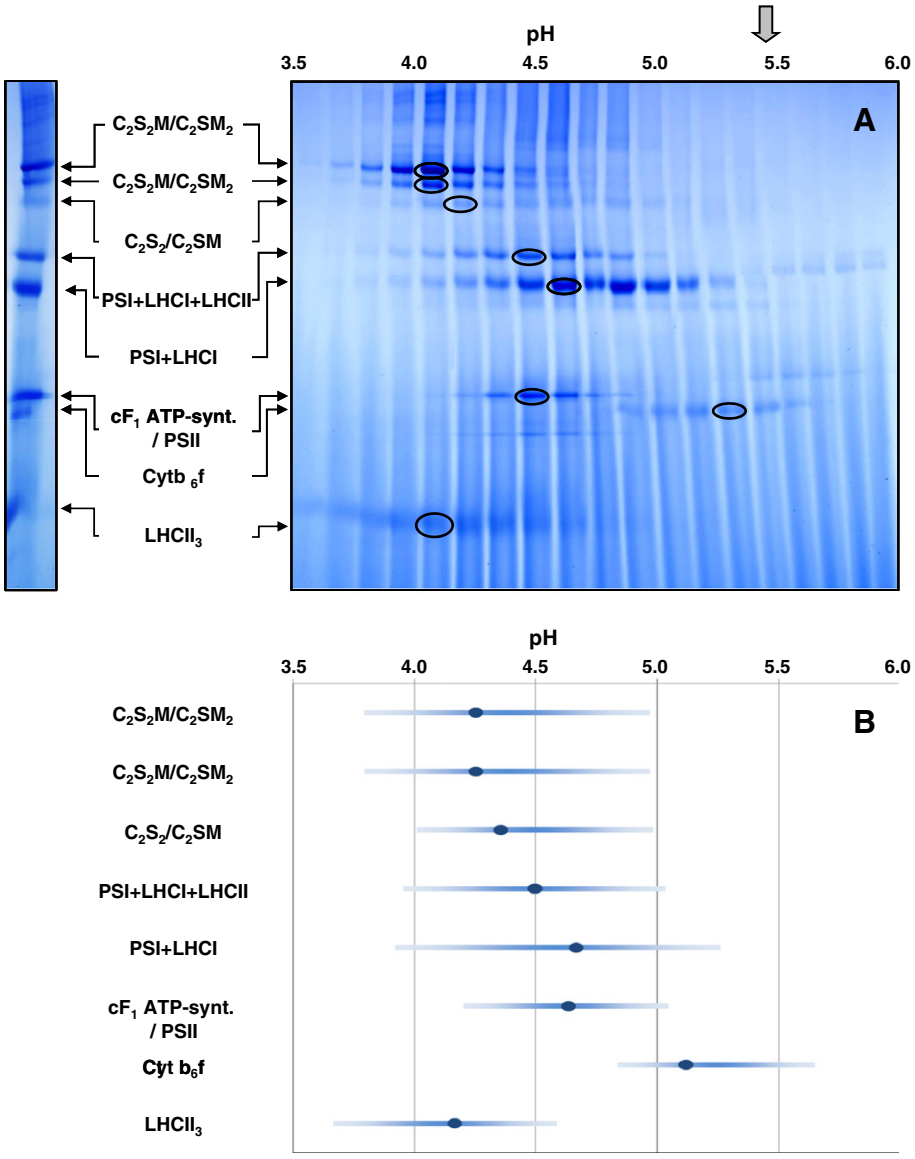

Fig. 4. Native pIs of chloroplast protein complexes and supercomplexes derived from nIEF-FFE (pH 2–8). A: Representative BN-PAGE of protein complexes of chloroplasts in the FFE fractions. Corresponding pH (taken at separation temperature) is indicated on top of the gels. Identities of complexes (determined by mass spectrometry; Suppl. Table 5) are given to the left of the gels (nomenclature of chloroplast supercomplexes in accordance with Heinemeyer et al. [59]): $C_2S_2M_2$, C_2S_2M/C_2SM_2, C_2S_2,C_2SM, supercomplexes of dimeric photosystem II reaction centre (C2) and varying number of strongly (S) and moderately (M) bound light-harvesting complex II trimers; PSI + LHCI + LHCII, supercomplex of photosystemI I and light-harvesting complex I with attached light-harvesting complex II; PSI + LHCI, supercomplex of photosystem I and light-harvesting complex I; cF_1 ATP-synt., F_1 part of chloroplast ATP-synthase; PSII, photosystem II; Cyt b_6f, Cytochrome b_6f complex; LHCII, trimeric light-harvesting complex II. Peak bands of complexes and supercomplexes are encircled; the grey arrow on the top indicates the horizontal position of the sample injection point. B: Schematic view of the distribution pattern of peak npI (dark blue spots) and npI range (light blue bars) of chloroplastic protein complexes and supercomplexes. Mean values of three individual plastid preparations and FFE separations according to the mean values given in Table 2 are shown.

for biological reasons or related to the experimental setup, can be expected to exert a strong influence on the protein complexes. Likewise, we only know little about the use of isoforms within these complexes. Mass spectrometry has the potential to reveal use of different isoforms, for example of LHCII subunits across the FFE fractions. However, in practical terms this often proves difficult since such isoforms share amino acid sequences for many of their tryptic peptides, making it difficult to detect such homologs. LHCII is known for its variable subunit composition and therefore formation of several homo- and heterotrimers were observed under in-vitro conditions [31]. Unfortunately, detailed analyses of LHCII across several FFE fractions revealed no difference in isoform use (data not shown). However, this does not necessarily mean that isoform use can be excluded. Rather, it is not detectable under the conditions applied here.

The influence on solubilisation of protein complexes by digitonin on their isoelectric points cannot be quantified by our data. It has been shown, that in gel-based systems the use of low detergent/protein ratios led to protein complexes migrating slower than it was the case with higher amounts. This effect has not only been observed for digitonin, but also for other detergents, such as Triton X100 and n-dodecylmaltoside [38]. Most likely, lower amounts of detergent are less efficient in removing lipids from the protein complexes which impacts their apparent molecular masses. To our knowledge, nothing is known about the influence this might have on the pI of the protein complexes. Nevertheless, the charged, hydrophilic parts of the lipid molecules are facing the aqueous solution and can therefore be expected to exert some influence on the protein complexes pI. Interestingly, streaking seems to be more pronounced in the chloroplast samples.

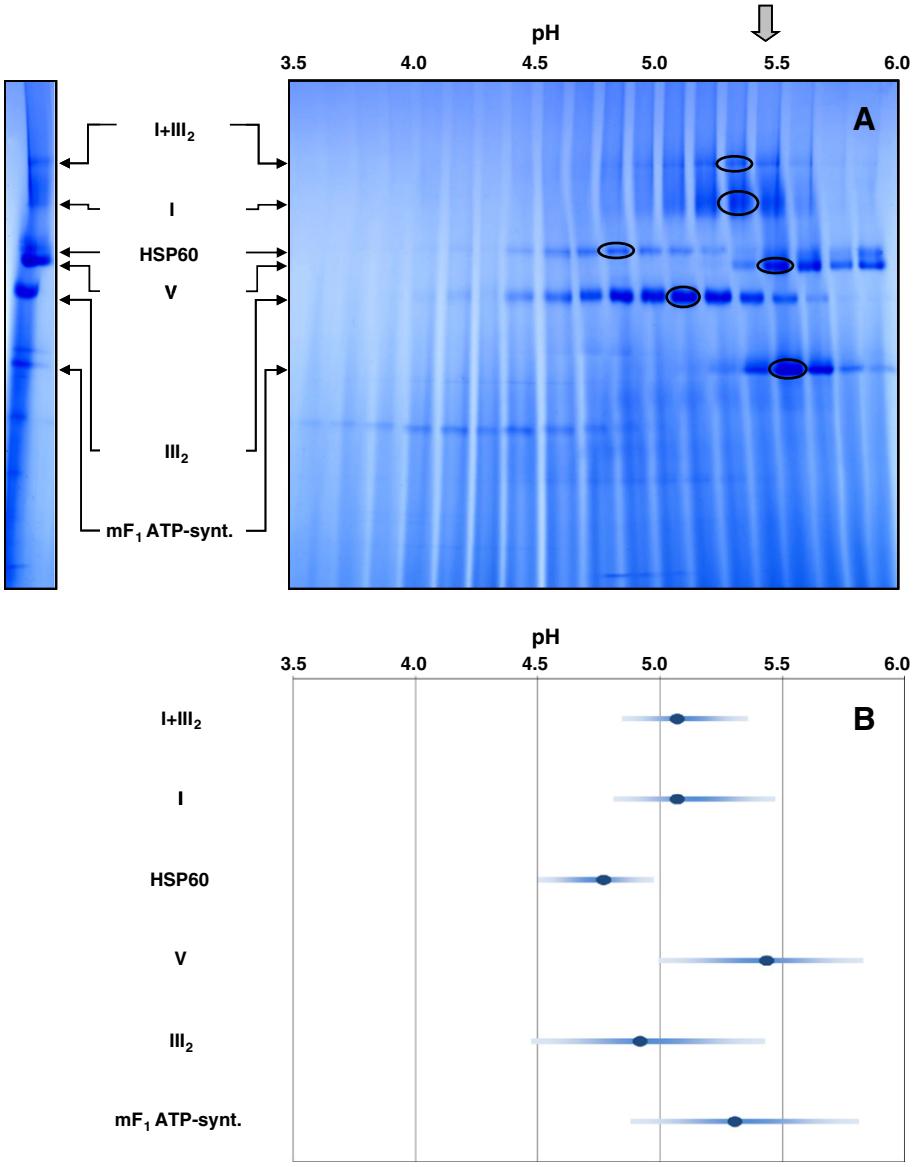

Fig. 5. Native pIs of mitochondrial protein complexes and supercomplexes as determined by nIEF-FFE (pH 2–8). A: Representative BN-PAGE of protein complexes of mitochondria in the FFE fractions. Corresponding pH (taken at separation temperature) is indicated on top of the gels. Identities of complexes (determined by mass spectrometry; Suppl. Table 5) are given to the left of the gels: I + III_2, supercomplex formed of dimeric cytochrome c reductase and NADH dehydrogenase; I, NADH dehydrogenase; HSP60, heat-shock protein 60; V, mitochondrial ATP-synthase; III_2, dimeric cytochrome c reductase; mF_1 ATP-synt., F_1 part of mitochondrial ATP-synthase. Peak bands of complexes and supercomplexes are encircled; the grey arrow on the top indicates the horizontal position of the of the sample injection point. B: Schematic view of the distribution pattern of peak npI (dark blue spots) and npI range (light blue bars) of chloroplastic protein complexes and supercomplexes. Mean values of three individual plastid preparations and FFE separations according to the mean values given in Table 2 are shown.

Underlying reasons for this are subject to speculation but the solubilisation efficiency of digitonin might differ between the two organelles since the composition of the inner mitochondrial membrane and the thylakoid membrane is not the same. Streaking could also be related to higher turnover/repair rates of photosynthetic complexes due to photo-damage or to different degrees of modifications on the proteins.

While the first two points affecting focussing of protein complexes during FFE cannot be confirmed or excluded easily, data from this and other studies indicate that the observed smearing is not an artefact. Typical reasons for streaking are incomplete focussing and excessive sample loading, which both do not seem to apply here since higher voltages did not improve definition. As can be seen in Suppl. Fig. 8, the FFE pH gradients were verging on linearity in the pH range used for focusing of the protein complexes, indicating ideal separating conditions. Also, standard error for each fraction was low, suggesting high reproducibility. FFE-performance was also good when compared to other studies. The low molecular mass proteins cytochrome c and myoglobin were each found in three to four FFE-fractions in native IEF-FFE of a mixture containing only four proteins [66]. On the same note, matrix free IEF of photosynthetic protein complexes using a different approach to the one described in this study also resulted in no clear focusing of protein complexes [64].

Smearing of protein complexes and supercomplexes over several FFE fractions and the manual inspection of this on BN-gels bears the risk of assigning peak fractions not solely due to the rise and fall of the target protein complex, but also due to the presence of another complex with the same molecular weight and similar npI in the background. In order to check this, MS data of the peak fraction of LHCII trimer, dimeric complex III and the mitochondrial and chloroplast F1 subcomplex were inspected closely. For the LHCII trimer, strong

Table 2
pH range and peak pH of protein membrane supercomplexes and complexes resolved by nIEF-FFE and subsequent BN-PAGE (Fig. 3).

(Super-)complex	Range of npI [pH][a]	npI peak fraction [pH][a]	Previously reported npI [pH]
$C_2S_2M_2$	3.79 (±0.11) to 4.97 (±0.26)	4.25 (±0.05)	
C_2S_2M/C_2SM_2	3.79 (±0.11) to 4.97 (±0.26)	4.25 (±0.05)	
C_2S_2/C_2SM	4.01 (±0.11) to 4.98 (±0.04)	4.36 (±0.04)	
PSI + LHCI + LHCII	3.95 (±0.07) to 5.03 (±0.15)	4.50 (±0.04)	
PSI + LHCI	3.92 (±0.08) to 5.26 (±0.11)	4.67(±0.03)	4.62 (spinach); D'Amici et al. [64]
cF_1 ATP-synthase/ PSII	4.20 (±0.05) to 5.05 (±0.14)	4.63(±0.06)	4.62 (PSII, spinach); D'Amici et al. [64]
Cyt b_6f	4.84 (±0.11) to 5.65 (±0.19)	5.12 (±0.09)	4.62 (spinach); D'Amici et al. [64]
LHCII	3.66 (±0.07) to 4.59 (±0.08)	4.17 (±0.03)	3.85–4.31 (spinach); D'Amici et al. [64] 4.20–4.42 (spinach); Jackowski et al. [63] 4.0–4.10 (*Arabidopsis*); Jackowski et al. [48]
$I + III_2$	4.85 (±0.14) to 5.36 (±0.11)	5.07 (±0.17)	
I	4.81 (±0.10) to 5.47 (±0.14)	5.07 (±0.17)	
HSP60	4.50 (±0.15) to 4.98 (±0.07)	4.77 (±0.14)	
V	5.00 (±0.01) to 5.83 (±0.05)[b]	5.44 (±0.03)	
III_2	4.48 (±0.18) to 5.43 (±0.18)	4.92 (±0.13)	
mF_1 ATP-synthase	4.88 (±0.25) to 5.82 (±0.09)	5.31 (±0.17)	

[a] Mean value and standard error of three (chloroplasts) or two (mitochondria) individual replicates.
[b] Not shown on gel in Fig. 4.

signals of other protein complexes and proteins (ATP synthase, fructose bisphosphate aldolase) were found alongside the LHCII proteins (Suppl. Table 5). To test if the presence of these proteins influenced the assessment of the npI of the LHCII trimer, we performed another BN-gel of chloroplast FFE fractions, this time without Coomassie colloidal staining (Suppl. Fig. 9). Instead, we solely relied on the intrinsic chlorophyll stain of LHCII to establish the peak fraction of LHCII. It was found that the chlorophyll derived peak npI exactly matches that of the corresponding Coomassie stained gel exactly (Suppl. Fig. 6A). This clearly shows that the peak observed in the Coomassie stained gel is due to LHCII and not the other proteins observed in these fractions. Judging by the Mascot scores and sequence coverages of the identified proteins, abundances of non-target protein complex subunits or proteins are only minor for the other protein complexes with calculated npI (Suppl. Table 5).

Theoretically, the banding observed on the BN gels could also be the product of dissociation of stoichiometrically inchoate assemblies of protein complexes. After solubilisation, such supercomplexes stable under FFE-conditions could have been focussed according to npI but fell apart under the (potentially) higher stresses imposed on them during BN-PAGE. Mechanical forces acting of the complexes during electrophoresis as well as the influence on the negatively charged Coomassie dye may affect the stability of supramolecular interactions. Strikingly, peak broadening was observed for mitochondria and chloroplasts alike. The strain put on the supercomplexes during BN-PAGE therefore needs to be considerably higher than in the matrix-free FFE. However, the potential of BN-PAGE to retain supramolecular structures is well documented. Mitochondrial protein supercomplexes separated by sucrose density centrifugation clearly did not dissociate during BN-PAGE [67]. Sucrose density centrifugation is also a matrix-free approach not employing Coomassie and, compared to FFE, might be considered even better suited to retain native structures due to the lack of an electric field. Therefore, if no dissociation of supercomplexes in BN-PAGE can be detected after sucrose density centrifugation, it seems very unlikely that such should be the case after FFE.

In summary, smearing of protein complexes most likely can be attributed to intrinsic variations of charges, solubilisation effects, or both. At the same time, artificial causes can largely be excluded.

2.6. Calculated and empiric npIs of membrane protein complexes and supercomplexes involved in plant energy metabolism

In order to assess concordance of our approaches, the calculated npIs for trimeric LHCII, dimeric complex III, as well as the mitochondrial and chloroplast F_1 subcomplexes were compared to the pH of the peak nIEF-FFE fractions of the corresponding protein complexes on the BN-gels. For LHCII, a deviation of up to 0.2 pH points was observed between the experimental and calculated values, when the pK_a values suggested by Henriksson et al. [27] were used on the surface exposed residues only.

The dimeric mitochondrial complex III showed a peak npI of 4.92 in the FFE, differing more than 0.7 pH units from our prediction of 5.6. Most likely, the prediction of surface exposed ionisable amino acids using the bovine structure model was too inaccurate due to the high phylogenetic distance between the bovine and Arabidopsis proteins, which compromised prediction accuracy. Likewise, mitochondrial F_1 ATP-synthase showed a peak npI of 5.31 differing 0.7 to 0.8 pH units from the predicted value of 4.56. This deviation very likely is caused by additional subunits remaining attached to the Arabidopsis F_1-subcomplex after solubilisation. In fact, MS analysis of the peak fraction revealed four additional subunits (Suppl. Table 5): a, b and the plant specific ATP17 and 6 kDa subunits which are believed to be involved in the F_o-part of ATP-synthase in plants. The presence of such subunits has been documented frequently in studies related to mitochondrial F_1: Hamasur and Glaser found OSCP in preparations of F_1 ATP-synthase of spinach [68]; an 8 kDa subunit was reported to be present in mitochondrial F_1-ATP-synthase of potato by Jänsch et al. [69]. Additionally, in the mitochondrial complex proteome of *Arabidopsis thaliana* [70], subunit b was found in spots corresponding to the F_1-part. The gentle solubilisation methods used in the above-mentioned studies and in our own approach might facilitate the existence of mitochondrial F_1 ATP-synthase complexes with subunits of F_o origin. These subunits potentially increase the npI of the solubilised F_1 subcomplex in the same way the c-subunits of the yeast structure have done it in the npI calculation with PROPKA 2.0. Interestingly, for the plastid F_1 additional subunits were not found to the same extend, which could explain the good correlation between calculated and experimentally derived npIs.

Prediction of chloroplast F_1 ATP-synthase npI was complicated by the low homology of δ and ε subunits between yeast mitochondrial and Arabidopsis chloroplastic F_1 ATP-synthase. Nevertheless, focussing on the water-accessible ionisable residues on the surface of the complex for the calculation of npI resulted in a predicted npI of 4.70, which is only 0.07 pH units away from the experimentally derived peak npI (4.63).

These results imply that the contribution of surface exposed, water-accessible ionisable amino acids is the main feature influencing the npIs of proteins and protein complexes of the chloroplast and mitochondrial membrane. In case of the LHCII complex, the high similarity of pea and Arabidopsis LHCII amino acid sequences enabled a good identification of water accessible ionisable amino acids in Arabidopsis which is also reflected in a good agreement between the calculated and experimentally derived values. Chloroplast F_1 ATP-synthase showed a similar close gap between predicted and experimental derived npI despite the more difficult alignment of subunits. The

divergence in calculated and experimental npI observed for the mitochondrial complexes most likely is due to high phylogenetic distances between Bos / yeast and Arabidopsis and/or due to the presence of additional subunits of the F_1 ATP-synthase in our preparation.

3. Conclusions

Despite the progress made in the prediction of pK_a values of amino acids in native proteins, the prediction estimation of native isoelectric points remains challenging. In this study we present results of a rather simple prediction method based on the Hendersson-Hasselbalch equation. Publicly available homologous structures combined with sequence alignments for the identification of surface exposed, water accessible amino-acids produced results which are close to experimentally derived native pIs. Our predictions based on highly similar and phylogenetically more distant structures clearly indicate that cross species npI predictions are feasible with this approach given that the degree of structural homology between target species and matrix species is reasonably high. Experimental assessment of npIs was conducted using nIEF-FFE to preserve the native state of solubilised membrane protein (super-) complexes of chloroplasts and mitochondria without aggregation and precipitation. Native IEF-FFE also allowed isoelectric focussing of chloroplasts membrane protein complexes up to 1500 kDa for the first time. Most likely, this is due to the use of digitonin instead of the ubiquitously used n-dodecylmaltoside, which destabilises most supercomplexes. To our knowledge, no experimental npI data are available for plant mitochondrial complexes and supercomplexes to date, while data on the chloroplast protein complexes and supercomplexes is extended by this study. In general, the membrane protein complexes of chloroplasts have a more acidic npI compared to the mitochondrial ones. Furthermore, the empiric npIs of LHCII and complex III of Arabidopsis are more acidic than most calculation methods suggest. Unfortunately, for Arabidopsis, crystal structures for energy-related protein complexes from closely related species are scarce. We therefore conclude that the experimental validation of native pIs remains the gold standard.

4. Materials and methods

4.1. Protein structures and pI calculations

The structures of trimeric LHCII from *Pisum sativum* (PDB ID: 2bhw) [4], dimeric mitochondrial complex III from *Bos taurus* (PDB ID: 1pp9) [35] and yeast mitochondrial F_1F_o ATP-synthase [42] were acquired from the PDB (www.pdb.org) [71]. The missing 6.4 kDa subunit in 1pp9 was taken from a different structure of bovine complex III (PDB ID: 1l0l) [36]. Furthermore, the structure of *E. coli* δ-subunit of F_1 ATP-synthase resolved by Wilkens et al. [72] was retrieved from PDB (PDB-ID: 2a7u). Amino acids with ionisable side chains exposed to a water accessible surface were selected using the Jmol software [28] using a surface probe of 1.4 Å in diameter. First, all amino acids with contact to the probe were recorded manually. Next, using NetsurfP1.1 [30], amino acids buried by more than 75% within the polypeptide structure were excluded from the list (conditions: cut off value 25%, each subunit was treated as a secondary structure protein). Subsequently, remaining residues (including N/C-termini) were assigned to lumen/stroma or matrix/intracristal space sides, respectively. Residues enclosed in the membrane bilayer were excluded from further calculations. Amino acid sequences of homologous subunits of *Arabidopsis thaliana* LHCII (P0CJ48, Q9SHR7, Q9S7M0), complex III (Q42290, Q9ZU25, P42792, Q9FKS5, Q9LYR2, Q9SUU5, Q0WWE3, Q9SG91, Q9LXJ2, Q94K78), mitochondrial F_1 ATP-synthase (P92549, P83484, Q96250, Q96252, Q96253) and chloroplast F_1 ATP-synthase (P56757, P19366, Q01908, Q9SSS9, P09468) were obtained from the UniProt database [73]. Transit peptides were removed from polypeptide sequences according to experimental data stored in the UniProt database. Alternatively, the length of the transit peptide was predicted by TargetP1.1 [33] using a reliability class of ≤3. Similar to pea, Bos and yeast, exposed Arabidopsis residues were calculated using NetsurfP1.1 with the same parameters indicated above. Alignments of pea/beef and Arabidopsis subunits were performed by Genedoc [74] applying the Blossum 62 matrix with settings as follows: const cost = 20, gap open cost = 8, gap extent cost = 4. The resulting final set of amino acid residues together with the N/C-terminal charges and the location data from the alignment were used to calculate npIs of whole protein complexes, or their liquid phase exposed surface only. The calculation itself was done using a self-developed tool, 'nativepI' (http://www.genetik.uni-hannover.de/nativepI.html), which is based on the source-code by Lukasz Kozlowski [47]. Modifications allow the implementation of multiple C- and N-termini. pK_a values either optimised for native proteins [27] or for denatured, linearised proteins as used by the EMBOSS software package [46] were applied. Calculations were also performed for all amino acids of the peptide sequence, except for those found in transit peptides.

An alternative approach to npI calculation based on structural information is the PROPKA2.0 [50] software tool. It was used to calculate the npI of pea LHCII, bovine complex III, and yeast F_1 ATP-synthase (including the F_O-rotor) only since the lack of Arabidopsis structures prohibited its use. In the case of missing residues in complex III PBD structures which denied the calculation of its npI, the output graph was used to estimate the npI.

4.2. Plant material and preparation of organelles

Arabidopsis thaliana ecotype Columbia-0 plants were grown for 6 weeks under 130 µmol/m^2/s of light (8 h/day) at 23/18 °C (day/night). Chloroplast isolation was performed according to Aronsson and Jarvis [75] with minor modifications to improve yield: 200 g of leaves were ground with mortar and pestle in batches of approx. 50 g, using 400 ml of isolation buffer in total. Sea sand was added to improve disruption of the material. The homogenate was centrifuged at 300 g and 4 °C for 1 min. The supernatant was centrifuged for 5 min at 1000 g and 4 °C. The resulting supernatant was discarded and the pellet was resuspended in 36 ml of isolation buffer. 3 ml of sample was loaded on each of twelve two-step percoll gradients comprised of 7 ml bottom layer and 15 ml of top layer. Quantitation of isolated chloroplasts was based on chlorophyll concentration according to Porra et al. [76].

An *Arabidopsis thaliana* ecotype Columbia-0 cell culture cultivated as described by Sunderhaus and co-workers [77] was used for mitochondria isolations by a procedure described elsewhere [78].

4.3. Native isoelectric focussing free-flow electrophoresis

Native isoelectric focussing was carried out in a BD Free Flow Electrophoresis system (Becton, Dickinson & Company, Franklin Lakes, USA) using a separation chamber height of 0.4 mm. Anodic stabilisation medium (inlet 1) contained 100 mM H_2SO_4, 250 mM Taurine and 50 mM alpha-Hydroxyisobutric acid in counter-flow medium (25% [w/v] Glycerol and 0.08% [w/w] HPMC), pH 1.2. Cathodic stabilisation medium (inlet 7) was made of 150 mM NaOH, 50 mM Ethanolamine, 250 mM Glycine and 50 mM AMPSO in counter-flow medium, ph 9.5. Separation medium (inlets 2–6) was prepared of 0.5 % [w/w] Servalytes pH 2–4, 0.5% [w/w] Servalytes 4–6, 0.5% [w/w] Servalytes pH 6–8, 0.375% [w/w] Servalytes ph 3–10 (Serva Electrophoresis, Heidelberg, Germany) and 0.2% [w/w] digitonin (Sigma-Aldrich, St. Louis, USA ~50% purity) in counter-flow medium. Anode and cathode stabilisation media as well as separation medium were injected at a rate which resulted in a total flow of 60 ml h^{-1} and a perambulation time of approx. 20 minutes. Counter flow medium was injected at a rate of 14 ml h^{-1}.

Membrane protein complexes of chloroplasts and mitochondria were solubilised in FFE-solubilisation buffer (10 mM HEPES, 20 mM KCl, 10 mM $MgCl_2$, 10% [v/v] glycerol, pH 7.4) containing 5% [w/v] digitonin at a chlorophyll-detergent ratio of 1:50 for chloroplasts and a protein–detergent ratio of 1:5 for mitochondria. After 20 min on ice, solubilised complexes were centrifugation at 4 °C and 18000 g for 10 min. Solubilised membrane protein complexes were then diluted 1:1 with separation medium. Two percent [v/v] SPADNS-solution (Becton, Dickinson & Company, Franklin Lakes, USA) was added and the sample (with a protein concentration 2–4 $\mu g\ \mu l^{-1}$ for mitochondria and chloroplast proteins corresponding to 0.5 $\mu g\ \mu l^{-1}$ chlorophyll) and injected into the separation chamber at a rate of 1000 $\mu l\ h^{-1}$. For chloroplasts, in approximately 30 minutes a protein load equivalent to 250 μg chlorophyll has been subjected to FFE per run. For mitochondria, a total of 1–2 mg protein was loaded in the same amount of time.

Continuous native isoelectric focussing was carried out at 800 V (resulting in 28–30 mA) at 5–7 °C and FFE-fractions were collected in 96 well-plates. The pH of the fractions at separation temperature were measured using a Sentron MICRO pH electrode (Sentron, Roden, The Netherlands) in the 96-well-plates to determine the npI of the membrane protein complexes. From fraction 25 to 58 each fraction´s pH was independently measured three times. Below fraction 25 and above fraction 58, every second fraction was measured independently for three times.

Native isoelectric focussing free-flow electrophoresis was carried out three times for chloroplasts and two times for mitochondria. Each separation was done with different batches of isolated organelles.

5. BN-PAGE and mass-spectrometry

All selected fractions were submitted to high-resolution BN-PAGE (100 μl each) as described by Wittig et al. [79] or separated on precast BN mini-gels (Life Technologies, Darmstadt, Germany). Coomassie Brilliant Blue colloidal staining [80] was used to visualise protein bands on the gels.

Bands corresponding to peak fractions were analysed by mass-spectrometry as outlined by Klodmann et al. [70] with minor modifications to adjust the procedure for samples derived from BN-PAGE. In brief, tryptic peptides were generated in the presence of 1 μl of ProteaseMAX™ (Promega, Madison, USA). Extracted peptides were collected in 20 μl of LC sample buffer (2% [v/v] acetonitrile, 0.1% [v/v] formic acid) and subsequently 15 μl were submitted to mass-spectrometry using an EasynLC system (Proxeon, Thermo Scientific, Dreieich, Germany) coupled to a micrOTOF Q II MS (Bruker Daltonics, Bremen, Germany). LC separation was carried out using a 2 cm C18 precolumn, followed by a 10 cm C18 analytical column. Peptides were eluted from the column in a three step water/acetonitrile gradient (containing 0.1% [v/v] formic acid) with increasing acetonitrile concentrations (5% to 95% within 33 minutes). Up to three peptides were automatically selected for MS/MS fragmentation if their intensities exceeded 3000 counts in the precursor scan. Data analysis was done with ProteinScape 2.1 (Bruker Daltonics, Bremen, Germany) using the Mascot software (Matrix Science, London, UK) searching against the TAIR10 database (www.arabidopsis.org). Parameters were set as follows: Enzyme, trypsin/P; global modification, carbamidomethylation (C); variable modifications, acetyl (N), oxidation (M), up to 1 missing cleavage allowed; precursor ion mass tolerance, 25 ppm; fragment ion mass tolerance, 0.05 Da; peptide charge, 1+, 2+, 3+; instrument, ESI QUAD TOF; minimum peptide length, 4; Mascot score, >30.

Acknowledgements

We thank Dr. Nir Keren, Hebrew University of Jerusalem for cooperation, Michael Senkler for expert help in setting up nativepI and Marianne Langer for expert technical assistance. This joint research project was financially supported by the State of Lower-Saxony and the VolkswagenFoundation, Hannover, Germany (Project VWZN2326).

Appendix A. Supplementary data

Supplementary data to this article can be found online at http://dx.doi.org/10.1016/j.bbamem.2012.11.028.

References

[1] S.B. Petersen, P.H. Jonson, P. Fojan, E.I. Petersen, M.T. Petersen, S. Hansen, R.J. Ishak, E. Hough, Protein engineering the surface of enzymes, J. Biotechnol. 66 (1998) 11–26.
[2] B. Honig, A. Nicholls, Classical electrostatics in biology and chemistry, Science 268 (1995) 1144–1149.
[3] E.D. Getzoff, D.E. Cabelli, C.L. Fisher, H.E. Parge, M.S. Viezzoli, L. Banci, R.A. Hallewell, Faster superoxide dismutase mutants designed by enhancing electrostatic guidance, Nature 358 (1992) 347–351.
[4] J. Standfuss, A.C. van Terwisscha Scheltinga, M. Lamborghini, W. Kühlbrandt, Mechanisms of photoprotection and nonphotochemical quenching in pea light-harvesting complex at 2.5 Å resolution, EMBO J. 24 (2005) 919–928.
[5] L. Serrano, A. Horovitz, B. Avron, M. Bycroft, A.R. Fersht, Estimating the contribution of engineered surface electrostatic interactions to protein stability by using double-mutant cycles, Biochemistry 29 (1990) 9343–9352.
[6] E. Alexov, Numerical calculations of the pH of maximal protein stability, Eur. J. Biochem. 271 (2004) 173–185.
[7] G. von Heijne, Membrane-protein topology, Nat. Rev. Mol. Cell Biol. 7 (2006) 909–918.
[8] A.J. Russell, A.R. Fersht, Rational modification of enzyme catalysis by engineering surface charge, Nature 328 (1987) 496–500.
[9] S. Ferguson-Miller, G.T. Babcock, Heme/Copper Terminal Oxidases, Chem. Rev. 96 (1996) 2889–2908.
[10] R. Schwartz, C.S. Ting, J. King, Whole proteome pI values correlate with subcellular localizations of proteins for organisms within the three domains of life, Genome Res. 11 (2001) 703–709.
[11] M.J.E. Sternberg, F.R.F. Hayes, A.J. Russell, P.G. Thomas, A.R. Fersht, Prediction of electrostatic effects of engineering of protein charges, Nature 330 (1987) 86–88.
[12] K.A. Kantardjieff, B. Rupp, Protein isoelectric point as a predictor for increased crystallization screening efficiency, Bioinformatics 20 (2004) 2162–2168.
[13] M.J. Mizianty, L. Kurgan, Sequence-based prediction of protein crystallization, purification and production propensity, Bioinformatics 27 (2011) i24.
[14] B. Bjellqvist, G.J. Hughes, C. Pasquali, N. Paquet, F. Ravier, J.C. Sanchez, S. Frutiger, D. Hochstrasser, The focusing positions of polypeptides in immobilized pH gradients can be predicted from their amino acid sequences, Electrophoresis 14 (1993) 1023–1031.
[15] B. Skoog, A. Wichman, Calculation of the isoelectric points of polypeptides from the amino acid composition, TrAC Trends Anal. Chem. 5 (1986) 82–83.
[16] A. Sillero, J. Ribeiro, Isoelectric points of proteins: Theoretical determination, Anal. Biochem. 179 (1989) 319–325.
[17] D.G. Isom, C.A. Castaneda, B.R. Cannon, E.B. Garcia-Moreno, Large shifts in pKa values of lysine residues buried inside a protein, Proc. Natl. Acad. Sci. 108 (2011) 5260–5265.
[18] W.R. Forsyth, J.M. Antosiewicz, A.D. Robertson, Empirical relationships between protein structure and carboxyl pKa values in proteins, Proteins 48 (2002) 388–403.
[19] M.H.M. Olsson, Protein electrostatics and pKa blind predictions; contribution from empirical predictions of internal ionizable residues, Proteins 79 (2011) 3333–3345.
[20] H. Li, A.D. Robertson, J.H. Jensen, Very fast empirical prediction and rationalization of protein pKa values, Proteins 61 (2005) 704–721.
[21] M.H.M. Olsson, C.R. Søndergaard, M. Rostkowski, J.H. Jensen, PROPKA3: Consistent Treatment of Internal and Surface Residues in Empirical pK_a Predictions, J. Chem. Theory Comput. 7 (2011) 525–537.
[22] T. Meyer, G. Kieseritzky, E.W. Knapp, Electrostatic pKa computations in proteins: Role of internal cavities, Proteins 79 (2011) 3320–3332.
[23] M.R. Gunner, X. Zhu, M.C. Klein, MCCE analysis of the pKas of introduced buried acids and bases in staphylococcal nuclease, Proteins 79 (2011) 3306–3319.
[24] V. Couch, A. Stuchebrukhov, Histidine in continuum electrostatics protonation state calculations, Proteins 79 (2011) 3410–3419.
[25] E. Bombarda, G.M. Ullmann, pH-dependent pKa values in proteins–a theoretical analysis of protonation energies with practical consequences for enzymatic reactions, J. Phys. Chem. B 114 (2010) 1994–2003.
[26] A.C. Lee, G.M. Crippen, Predicting p Ka, J. Chem. Inf. Model. 49 (2009) 2013–2033.
[27] G. Henriksson, A.K. Englund, G. Johansson, P. Lundahl, Calculation of the isoelectric points of native proteins with spreading of pKa values, Electrophoresis 16 (1995) 1377–1380.
[28] Jmol: an open-source Java viewer for chemical structures in 3D, http://www.jmol.org/.
[29] M.A. Lomize, A.L. Lomize, I.D. Pogozheva, H.I. Mosberg, OPM: Orientations of Proteins in Membranes database, Bioinformatics 22 (2006) 623–625.
[30] B. Petersen, T. Petersen, P. Andersen, M. Nielsen, C. Lundegaard, A generic method for assignment of reliability scores applied to solvent accessibility predictions, BMC Struct. Biol. 9 (2009) 51.
[31] J. Standfuss, W. Kühlbrandt, The Three Isoforms of the Light-harvesting Complex II: SPECTROSCOPIC FEATURES, TRIMER FORMATION, AND FUNCTIONAL ROLES, J. Biol. Chem. 279 (2004) 36884–36891.

[32] T. Barros, W. Kühlbrandt, Crystallisation, structure and function of plant light-harvesting Complex II, Biochim. Biophys. Acta (BBA) - Bioenerg. 1787 (2009) 753–772.
[33] O. Emanuelsson, S. Brunak, G. von Heijne, H. Nielsen, Locating proteins in the cell using TargetP, SignalP and related tools, Nat. Protoc. 2 (2007) 953–971.
[34] T. Kajander, P.C. Kahn, S.H. Passila, D.C. Cohen, L. Lehtiö, W. Adolfsen, J. Warwicker, U. Schell, A. Goldman, Buried Charged Surface in Proteins, Structure 8 (2000) 1203–1214.
[35] L.s. Huang, D. Cobessi, E.Y. Tung, E.A. Berry, Binding of the Respiratory Chain Inhibitor Antimycin to the Mitochondrial bc1 Complex: A New Crystal Structure Reveals an Altered Intramolecular Hydrogen-bonding Pattern, J. Mol. Biol. 351 (2005) 573–597.
[36] X. Gao, X. Wen, C. Yu, L. Esser, S. Tsao, B. Quinn, L. Zhang, L. Yu, D. Xia, The Crystal Structure of Mitochondrial Cytochrome bc1, Biochemistry 41 (2002) 11692–11702.
[37] H.P. Braun, U.K. Schmitz, The bifunctional cytochromec reductase/processing peptidase complex from plant mitochondria, J. Bioenerg. Biomembr. 27 (1995) 423–436.
[38] H. Eubel, E.H. Meyer, N.L. Taylor, J.D. Bussel, N. O'Toole, J.L. Heazlewood, I. Castleden, I.D. Small, S.M. Smith, A.H. Millar, New Insights into the Respiratory Chain of Plant Mitochondria. Supercomplexes and a Unique Composition of Complex II, Plant Physiol. 133 (2003) 274–286.
[39] D. Gonzalez-Halphen, M.A. Lindorfer, R.A. Capaldi, Subunit arrangement in beef heart complex III, Biochemistry 27 (1988) 7021–7031.
[40] C.A. Yu, J.Z. Xia, A.M. Kachurin, L. Yu, D. Xia, H. Kim, J. Deisenhofer, Crystallization and preliminary structure of beef heart mitochondrial cytochrome-bc1 complex, Biochim. Biophys. Acta (BBA) - Bioenerg. 1275 (1996) 47–53.
[41] G. Groth, E. Pohl, The structure of the chloroplast F1-ATPase at 3.2 A resolution, J. Biol. Chem. 276 (2001) 1345–1352.
[42] D. Stock, A.G. Leslie, J.E. Walker, Molecular Architecture of the Rotary Motor in ATP Synthase, Science 286 (1999) 1700–1705.
[43] C. Mellwig, B. Böttcher, A Unique Resting Position of the ATP-synthase from Chloroplasts, J. Biol. Chem. 278 (2003) 18544–18549.
[44] S. Hong, P.L. Pedersen, ATP synthases: insights into their motor functions from sequence and structural analyses, J. Bioenerg. Biomembr. 35 (2003) 95–120.
[45] Y.A. Ovchinnikov, N.N. Modyanov, V.A. Grinkevich, N.A. Aldanova, O.E. Trubetskaya, I.V. Nazimov, T. Hundal, L. Ernster, Amino acid sequence of the oligomycin sensitivity-conferring protein (OSCP) of beef-heart mitochondria and its homology with the delta-subunit of the F1-ATPase of Escherichia coli, FEBS Lett. 166 (1984) 19–22.
[46] P. Rice, I. Longden, A. Bleasby, EMBOSS: the European Molecular Biology Open Software Suite, Trends Genet. 16 (2000) 276–277.
[47] Lukasz Kozlowski, Calculation of protein isoelectric point, http://isoelectric.ovh.org/index.html.
[48] G. Jackowski, K. Kacprzak, S. Jansson, Identification of Lhcb1/Lhcb2/Lhcb3 heterotrimers of the main light-harvesting chlorophyll a/b-protein complex of Photosystem II (LHC II), Biochim. Biophys. Acta 1504 (2001) 340–345.
[49] S. Caffarri, R. Kouřil, S. Kereïche, E.J. Boekema, R. Croce, Functional architecture of higher plant photosystem II supercomplexes, EMBO J. 28 (2009) 3052–3063.
[50] D.C. Bas, D.M. Rogers, J.H. Jensen, Very fast prediction and rationalization of pKa values for protein–ligand complexes, Proteins 73 (2008) 765–783.
[51] M.N. Davies, C.P. Toseland, D.S. Moss, D.R. Flower, BMC Biochem. 7 (2006) 2006.
[52] M. Islinger, C. Eckerskorn, A. Völkl, Free-flow electrophoresis in the proteomic era: A technique in flux, Electrophoresis 31 (2010) 1754–1763.
[53] J.P. Dubacq, J.C. Kader, Free flow electrophoresis of chloroplasts, Plant Physiol. 61 (1978) 465–468.
[54] H. Zischka, G. Weber, P.J.A. Weber, A. Posch, R.J. Braun, D. Bühringer, U. Schneider, M. Nissum, T. Meitinger, M. Ueffing, C. Eckerskorn, Improved proteome analysis of *Saccharomyces cerevisiae* mitochondria by free-flow electrophoresis, Proteomics 3 (2003) 906–916.
[55] H. Eubel, C.P. Lee, J. Kuo, E.H. Meyer, N.L. Taylor, A.H. Millar, TECHNICAL ADVANCE: Free-flow electrophoresis for purification of plant mitochondria by surface charge, Plant J. 52 (2007) 583–594.
[56] A. Völkl, H. Mohr, G. Weber, H.D. Fahimi, Isolation of peroxisome subpopulations from rat liver by means of immune free-flow electrophoresis, Electrophoresis 19 (1998) 1140–1144.
[57] H. Eubel, E.H. Meyer, N.L. Taylor, J.D. Bussell, N. O'Toole, J.L. Heazlewood, I. Castleden, I.D. Small, S.M. Smith, A.H. Millar, Novel Proteins, Putative Membrane Transporters, and an Integrated Metabolic Network Are Revealed by Quantitative Proteomic Analysis of Arabidopsis Cell Culture Peroxisomes, Plant Physiol. 148 (2008) 1809–1829.
[58] J. McDonough, E. Marbán, Optimization of IPG strip equilibration for the basic membrane protein mABC1, Proteomics 5 (2005) 2892–2895.
[59] J. Heinemeyer, H. Eubel, D. Wehmhöner, L. Jänsch, H.-P. Braun, Proteomic approach to characterize the supramolecular organization of photosystems in higher plants, Phytochemistry 65 (2004) 1683–1692.
[60] H. Schägger, G. von Jagow, Blue native electrophoresis for isolation of membrane protein complexes in enzymatically active form, Anal. Biochem. 199 (1991) 223–231.
[61] E.J. Boekema, H. van Roon, J.F. van Breemen, J.P. Dekker, Supramolecular organization of photosystem II and its light-harvesting antenna in partially solubilized photosystem II membranes, Eur. J. Biochem. 266 (1999) 444–452.
[62] R. Kouřil, J.P. Dekker, E.J. Boekema, Supramolecular organization of photosystem II in green plants, Biochim. Biophys. Acta (BBA) - Bioenerg. 1817 (2012) 2–12.
[63] G. Jackowski, K. Pielucha, Heterogeneity of the main light-harvesting chlorophyll a/b–protein complex of photosystem II (LHCII) at the level of trimeric subunits, J. Photochem. Photobiol. B: Biol. 64 (2001) 45–54.
[64] G.M. D'Amici, A.M. Timperio, L. Zolla, Coupling of Native Liquid Phase Isoelectrofocusing and Blue Native Polyacrylamide Gel Electrophoresis: A Potent Tool for Native Membrane Multiprotein Complex Separation, J. Proteome Res. 7 (2008) 1326–1340.
[65] N.V. Dudkina, R. Kouril, K. Peters, H.-P. Braun, E.J. Boekema, Structure and function of mitochondrial supercomplexes, Biochim. Biophys. Acta 1797 (2010) 664–670.
[66] S.A. Ouvry-Patat, M.P. Torres, H.-H. Quek, C.A. Gelfand, P. O'Mullan, M. Nissum, G.K. Schroeder, J. Han, M. Elliott, D. Dryhurst, J. Ausio, R. Wolfenden, C.H. Borchers, Free-flow electrophoresis for top-down proteomics by Fourier transform ion cyclotron resonance mass spectrometry, Proteomics 8 (2008) 2798–2808.
[67] N.V. Dudkina, H. Eubel, W. Keegstra, E.J. Boekema, H.P. Braun, Structure of a mitochondrial supercomplex formed by respiratory-chain complexes I and III, Proc. Natl. Acad. Sci. 102 (2005) 3225–3229.
[68] B. Hamasur, E. Glaser, Plant mitochondrial F0F1 ATP synthase. Identification of the individual subunits and properties of the purified spinach leaf mitochondrial ATP synthase, Eur. J. Biochem. 205 (1992) 409–416.
[69] L. Jansch, V. Kruft, U.K. Schmitz, H.-P. Braun, New insights into the composition, molecular mass and stoichiometry of the protein complexes of plant mitochondria, Plant J. 9 (1996) 357–368.
[70] J. Klodmann, M. Senkler, C. Rode, H.P. Braun, Defining the "protein complex proteome" of plant mitochondria, Plant Physiol. 157 (2011) 587–598.
[71] H.M. Berman, J. Westbrook, Z. Feng, G. Gilliland, T.N. Bhat, H. Weissig, I.N. Shindyalov, P.E. Bourne, The Protein Data Bank, Nucleic Acids Res. 28 (2000) 235–242.
[72] S. Wilkens, D. Borchardt, J. Weber, A.E. Senior, Structural characterization of the interaction of the delta and alpha subunits of the Escherichia coli F1F0-ATP synthase by NMR spectroscopy, Biochemistry 44 (2005) 11786–11794.
[73] The UniProt Consortium, Ongoing and future developments at the Universal Protein Resource, Nucleic Acids Res. 39 (2010) D214.
[74] K.B. Nicholas, H.B. Nicholas Jr., D.W. Deerfield II, Genedoc: Analysis and Visualization of Genetic Variation., embnet.news 4 (1997) 1–4, 1997.
[75] H. Aronsson, P. Jarvis, A simple method for isolating import-competent Arabidopsis chloroplasts, FEBS Lett. 529 (2002) 215–220.
[76] R.J. Porra, W.A. Thompson, P.E. Kriedemann, Determination of accurate extinction coefficients and simultaneous equations for assaying chlorophylls a and b extracted with four different solvents: verification of the concentration of chlorophyll standards by atomic absorption spectroscopy, Biochim. Biophys. Acta (BBA) - Bioenerg. 975 (1989) 384–394, (http://www.sciencedirect.com/science/article/pii/S0005272889803470).
[77] S. Sunderhaus, N.V. Dudkina, L. Jänsch, J. Klodmann, J. Heinemeyer, M. Perales, E. Zabaleta, E.J. Boekema, H.P. Braun, Carbonic anhydrase subunits form a matrix-exposed domain attached to the membrane arm of mitochondrial complex I in plants, J. Biol. Chem. 281 (2006) 6482–6488.
[78] W. Werhahn, A. Niemeyer, L. Jänsch, V. Kruft, U.K. Schmitz, H. Braun, Purification and characterization of the preprotein translocase of the outer mitochondrial membrane from Arabidopsis. Identification of multiple forms of TOM20, Plant Physiol. 125 (2001) 943–954.
[79] I. Wittig, H.P. Braun, H. Schägger, Blue native PAGE, Nat. Protoc. 1 (2006) 418–428.
[80] V. Neuhoff, N. Arold, D. Taube, W. Ehrhardt, Improved staining of proteins in polyacrylamide gels including isoelectric focusing gels with clear background at nanogram sensitivity using Coomassie Brilliant Blue G-250 and R-250, Electrophoresis 9 (1988) (1988) 255–262.